

Table 5. *The proportion of different types of molecular pairs occurring for pairs of neighbouring sites in BEMB1, compared with the proportion that would be present if each site were independently occupied by m_A molecules of type 1 and $(1-m_A)$ of type 2. The pair consists of the site listed together with the central site 55501*

Pair type	Site 66502	Site 65501	Site 56501	Random
1-1	0.262	0.279	0.320	0.314
1-2, 2-1	0.298	0.281	0.240	0.246
2-2	0.142	0.159	0.200	0.194

molecule and to carry out energy summations over a sufficiently large range of interaction distances. When this is done the results of the current experiment can be used together with the results from similar compounds to test such a theory.

We are grateful to K. Owen, M. Puza and G. Lockhart for technical assistance. One of us (JS) gratefully acknowledges the receipt of a Australian National University Scholarship during the tenure of which this work was carried out.

Acta Cryst. (1986). **B42**, 272-280

Three-Dimensional Structure of Yeast tRNA^{Asp}. I. Structure Determination

By M. B. COMARMOND,* R. GIEGÉ, J. C. THIERRY AND D. MORAS†

*Laboratoire de Cristallographie Biologique, Institut de Biologie Moléculaire et Cellulaire du CNRS,
15 rue René Descartes, 67084 Strasbourg CEDEX, France*

AND J. FISCHER

Laboratoire de Cristallographie, ERA 08, Institut Le Bel, 4 rue Blaise Pascal, 67070 Strasbourg CEDEX, France

(Received 5 October 1984; accepted 11 November 1985)

Abstract

The three-dimensional structure of yeast tRNA^{Asp}, an elongator tRNA with a short variable loop, has been solved to high resolution in two non-isomorphous but closely related orthorhombic crystal forms. A first attempt to solve the structure by molecular replacement using the molecular structure of yeast tRNA^{Phe} as a model was unsuccessful although the tRNA molecule could be correctly oriented within 10° by the rotation function. The phase problem was solved by the MIR approach. Two heavy-atom derivatives (Gd and Au) were used as markers. A 3.5 Å resolution map could thus be interpreted and a Kendrew skeletal model built. The folding of the molecule

is similar to that originally found for yeast tRNA^{Phe}. Major differences concern the relative positioning of the acceptor and anticodon stems: the more open conformation confers to the tRNA^{Asp} molecule a boomerang-like shape. Crystal packing involves self-complementary GUC anticodon interactions through a crystallographic twofold axis. This is the first visualization of such an interaction at the molecular level.

Introduction

Transfer ribonucleic acids (tRNA's) form a family of small nucleic acids (70-90 nucleotides) crucial for living cells. Their most extensively studied and best known function is their role in messenger RNA mediated protein synthesis where they act as 'adaptor molecules' (see the review in Schimmel, Söll &

* Present address: Immunologie Structurale, Institut Pasteur, 28 rue du Dr Roux, 75015 Paris, France.

† To whom reprint requests should be addressed.

References

- ABRAHAMS, S. C. & KEVE, E. T. (1971). *Acta Cryst.* **A27**, 157-165.
 BAHARIE, E. & PAWLEY, G. S. (1983). *J. Appl. Cryst.* **16**, 404-406.
 CENEDESE, P., BLEY, F. & LEFEBVRE, S. (1984). *Acta Cryst.* **A40**, 228-240.
 EPSTEIN, J. & WELBERRY, T. R. (1983). *Acta Cryst.* **A39**, 882-892.
 EPSTEIN, J., WELBERRY, T. R. & JONES, R. D. G. (1982). *Acta Cryst.* **A38**, 611-618.
 HAMILTON, W. C. (1965). *Acta Cryst.* **18**, 502-510.
 HAMILTON, W. C. & ABRAHAMS, S. C. (1970). *Acta Cryst.* **A26**, 18-24.
 HILL, R. J. & MADSEN, I. C. (1984). *J. Appl. Cryst.* **17**, 297-306.
 JOHNSON, C. K. (1976). *ORTEP II*. Report ORNL-5138. Oak Ridge National Laboratory, Tennessee.
 JONES, R. D. G. & WELBERRY, T. R. (1980). *Acta Cryst.* **B36**, 852-857.
 KITAIGORODSKII, A. I. (1973). *Molecular Crystals and Molecules*. New York: Academic Press.
 SAKATA, M. & COOPER, M. J. (1979). *J. Appl. Cryst.* **12**, 554-563.
 WELBERRY, T. R. (1983). *J. Appl. Cryst.* **16**, 192-197.
 WELBERRY, T. R. & GLAZER, A. M. (1985). *Acta Cryst.* **A41**, 394-399.
 WELBERRY, T. R. & JONES, R. D. G. (1980). *J. Appl. Cryst.* **13**, 244-251.
 WELBERRY, T. R., JONES, R. D. G. & EPSTEIN, J. (1982). *Acta Cryst.* **B38**, 1518-1525.
 WOOD, R. A., WELBERRY, T. R. & PUZA, M. (1984). *Acta Cryst.* **C40**, 1255-1260.

Abelson, 1979). Other functions, such as mRNA independent transfer of amino acids into different cellular components or participation in regulatory processes (regulation of biosynthesis of amino acids, aminoacyl-tRNA synthetase, tRNA, rRNA), have been characterized (La Rossa & Söll, 1980). The life cycle of tRNA and its various functions lead to interactions with many different proteins and nucleic acids. Some of these interactions have to be specific like the one with aminoacyl-tRNA synthetases, enzymes which attach the correct amino acid to their cognate tRNA's; some others, like the association with the elongation factors, are more general.

Our three-dimensional (3D) structural knowledge, at the atomic level, is essentially based on the pioneering studies on yeast tRNA^{Phe} which provided a general frame for all tRNA molecules (Quigley, Wang, Seeman, Suddath, Rich, Sussman & Kim, 1975; Sussman, Holbrook, Warrant, Church & Kim, 1978; Ladner, Jack, Robertus, Brown, Rhodes, Clark & Klug, 1975; Jack, Ladner & Klug, 1976; Stout, Mizuno, Rao, Swaminathan, Rubin, Brennan & Sundaralingam, 1978). Since then few other tRNA structures have been solved. Initiator tRNA^{Met} from yeast and *E. coli* have their 3D structure known to medium resolution (Schevitz, Podjarny, Krishnamachar, Hugues, Sigler & Sussman, 1981; Woo, Roe & Rich, 1980). The yeast tRNA^{Gly} structure, solved to 3.5 Å resolution, is unfortunately that of a denatured molecule (Wright, 1982). Yeast tRNA^{Asp} is the second elongator tRNA, which, due to the diffracting power of its crystals, enables a high-resolution study (Moras, Comarmond, Fischer, Weiss, Thierry, Ebel & Giegé, 1980). Its primary sequence, shown in Fig. 1, presents some features of interest when compared with that of tRNA^{Phe} (Gangloff, Keith, Ebel & Dirheimer, 1971). For instance, the number of G-C base pairs is exceptionally high, except in the D stem. Four G-U (ψ) base pairs are present. The variable loop is made of four nucleotides *versus* five in tRNA^{Phe}. Finally, the anticodon GUC is self-complementary assuming a slight mismatch at the uridine position. In this paper we give a full account of the studies which lead to the structure determination of yeast tRNA^{Asp} at the molecular level.

Structure determination

Crystallization and preliminary crystallographic data

tRNA^{Asp} was purified from brewer's yeast bulk tRNA by counter-current distribution followed by benzoylated DEAE-cellulose chromatography. Details of the crystallization procedure have already been published (Giegé, Moras & Thierry, 1977; Dock, Lorber, Moras, Pixa, Thierry & Giegé, 1984). The best crystals of a size suitable for diffractometer

Table 1. *Space group and cell parameters*

Interconversion between crystal forms can be achieved through temperature change (above 293 K *B* \rightarrow *A*) or by addition of Au salts (*A* \rightarrow *B*).

(A)	=	(B)
$a = 61.5 \text{ \AA}$		$a = 60.3 \text{ \AA}$
$b = 67.5$		$b = 68.0$
$c = 149.5$		$c = 149.5$

Space group: $C222_1$, $Z = 4$

measurements ($0.3 \times 0.3 \times 0.4$ mm) are obtained at room temperature (close to 293 K). Under these conditions two non-isomorphous but interconvertible crystal forms indistinguishable by their external shape are obtained. A detailed analysis of the crystalline transition has been published (Huong, Audry, Giegé, Moras, Thierry & Comarmond, 1984). In order to avoid cell-size fluctuation, all crystals were stabilized against 70% ammonium sulfate solutions before X-ray analysis. The solvent content of these crystals is close to 75%, a normal value for tRNA molecules.

The preliminary crystallographic data were determined on a precession camera. Subsequently, for each crystal used in data collection, cell parameters were refined by least-squares methods during the alignment procedure. The orientation matrix and the cell parameters were usually refined from the positions of sixteen carefully centered standard reflections. The values presented in Table 1 represent the mean value of the unit-cell parameters for each crystal form. The parameter c is quite constant whereas the fluctuation of the other two can reach 0.3 Å around the mean value.

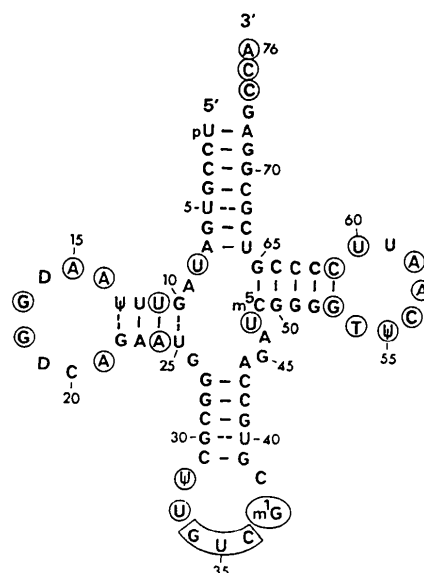


Fig. 1. The nucleotide sequence of yeast tRNA^{Asp}. For convenience the numbering system of the nucleotides is that of yeast tRNA^{Phe} (see Sprinzl & Gauss, 1984); in the 75-nucleotide-long tRNA^{Asp} position 47 in the variable loop has been omitted. Non-classical Watson-Crick base pairs are indicated by broken lines. Common nucleotides in most elongator tRNA's are circled.

Table 2. *Data reduction for crystal form A*

Derivative reflections are scaled to the native according to the formula $F = F_{\text{obs}} \times k \exp[B(\sin \theta/\lambda)^2]$. Only reflections for which $F > 2\sigma F$ are included.

$$wR = \left(\sum_{hkl} |w_{hkl} F_{hkl} - w_{hkl} \bar{F}_{hkl}| \right) / \sum_{hkl} w_{hkl} \bar{F}_{hkl} \text{ with } w = 1/\sigma^2.$$

Derivative	Observed reflections	Independent reflections	Agreement factors		Scaling parameters		Resolution (Å)
			R_{int}	wR	k	B	
Native A	8244 (two crystals)	5127	0.074	0.034	1	0	3.0
Gd ₂ (SO ₄) ₃	7422	4659	0.025	0.017	1.3	6.0	3.0
Au(en) ₂ Cl ₃	3652	1929	0.026	0.013	2.4	0.01	4.0
Lu ₂ (SO ₄) ₃ + Au(en) ₂ Cl ₃	5586	3126	0.032	0.018	2.2	6.7	3.5
Lu ₂ (SO ₄) ₃	3960	3114	0.013	0.011	1.5	5.7	3.5

Table 3. *Data reduction for crystal form B (see notes in Table 2)*

Derivative	Observed reflections	Independent reflections	Agreement factors		Scaling parameters		Resolution (Å)
			R_{int}	wR	k	B	
Native B	17440 (five crystals)	5262	0.054	0.026	1	0	2.9
Gd ₂ (SO ₄) ₃	4993	3975	0.038	0.018	1.08	3.3	3.0
Au(en) ₂ Cl ₃	4136	1773	0.032	0.021	2.7	-6.3	3.9
HgCl ₂	2586	1646	*	*	4.3	46	4.0
Gd ₂ (SO ₄) ₃ + Au(en)Cl ₃	4029	3477	0.025	0.013	2.5	6.7	3.5

* Values for the Hg derivative are not significant since only a few equivalent reflections have been measured.

Data collection

The diffracted intensities were collected at 291 and 297 K depending on the form on a four-circle Philips PW 1100 diffractometer specially modified for protein work (Fischer, Moras & Thierry, 1985). X-rays were produced by a sealed tube with a fine focus (0.4–0.8 mm) running at 1200 W. For the few largest crystals available (0.3 × 0.4 × 0.6 mm) the primary beam was filtered by a 9 μm thick nickel foil. For the smaller crystals (largest dimension <0.4 mm) we used a graphite monochromator to select the Cu Kα radiation. In this case the homogeneous part of the beam was better than 0.3 × 0.6 mm at the crystal level. Each reflection was measured using the ω scan and the flying step-scan procedure. This method involves a continuous scan of the angle with a transfer of the number of counts at regular time intervals corresponding to a step. Usually the peak was integrated over 0.5° with 0.03° steps. The angular speed varied from 0.016 to 0.032 s⁻¹ depending upon the size of the crystal.

tRNA^{ASP} crystals are heavily affected by X-ray exposure. The loss of diffracted intensities is usually of the order of 1% h⁻¹ at 3 Å resolution and 2 to 4 times less at 8 Å. To compensate for this effect each data set was collected in successive shells of decreasing resolution, the starting point being related to the quality of the crystal. In every case, data collection was stopped when the decay of the standard reflec-

tions measured every 2 h reached 30% of their starting value.

Data were processed as described by Fischer, Moras & Thierry (1985). Empirical absorption corrections were applied (North, Phillips & Mathews, 1968).

For form A of tRNA^{ASP}, the native data result from an averaging of the data of two crystals; for form B five crystals were used. For all the heavy-atom derivatives used in the MIR method only the data from the best crystals were kept. The results of the data-reduction process are summarized in Tables 2 and 3 respectively for forms A and B.

Molecular replacement

The expected similarity of the yeast tRNA^{ASP} structure to the canonical form found in tRNA^{Phe} prompted us to use the molecular-replacement method using the structure of yeast tRNA^{Phe} as a model.

The determination of the orientation of the known molecule in the unit cell was performed using the rotation-function approach, first introduced by Rossmann & Blow (1962). The programs were adapted to our PDP11 minicomputer from the original version of Crowther's (1972) rotation-function package.

Two data sets were used as model. The first was based on 671 observed structure factors (F_{obs}) of the orthorhombic form of yeast tRNA^{Phe} (data between

Table 4. *Rotation-function results*

Rotation functions were computed using Crowther's program. Two data sets were used for the tRNA^{Phe} model data: observed amplitudes of the orthorhombic form (F_{obs}) and calculated amplitudes from the high-resolution model of tRNA^{Phe} in a triclinic cell (F_c). The results are given for two sets of resolution (12-7 Å and 12-6 Å) and various radii of inspection (R). R_F stands for the rotation-function value.

Resolution (Å)	R (Å)	tRNA ^{Phe} triclinic			R_F	tRNA ^{Phe} orthorhombic			R_F
		θ_1 (°)	θ_2 (°)	θ_3 (°)		θ_1 (°)	θ_2 (°)	θ_3 (°)	
12-7	20	92.5	32.5	95	115				
		235	60	75	112				
		122.5	95	105	99				
	40	92.5	18	95	77				
		232.5	62	75	76				
		135	50	165	67				
12-6	15	95	35	95	136				
		230	50	85	123				
		105	110	110	105				
	20	90	35	95	108				
		237.5	60	75	105				
		152.5	100	95	95				
	25	90	45	95	100	90	35	90	62
		243	65	70	90	117.5	90	90	55
		97.5	80	-65	72	115	55	62.5	46
	30	92.5	15	90	66	90	40	77.5	68
		232.5	60	75	64	90	25	90	62
		87.5	45	95	60	120	55	60	61
	35	90	15	95	62				
		235	60	75	61				
		85	45	95	60				

12 and 6 Å resolution). The second data set (F_c) was calculated from the coordinates of the three-dimensional model of yeast tRNA^{Phe} in a triclinic cell. For structure factor computations the wybutine base was omitted; the removal of the 3'-terminal ACCA_{OH} end was also tested but appeared to be negligible in its consequences.

Systematic searches over all possible Eulerian angles were performed. Two parameters varied during the investigation: the resolution of the data and the radius of the overlapping vectors considered. A summary of the results is presented in Table 4. With both model data sets the best results are obtained with the 12-6 Å data set and a radius of inspection of 25 Å. The rotation function using the observed structure factor for both tRNA^{Asp} and tRNA^{Phe} gives a maximum of 62 for θ_1 , θ_2 and θ_3 , respectively equal to 90, 35 and 90°; the second and third peaks on the same function are at 55 and 46. With the triclinic model structure of tRNA^{Phe} a peak of 100.1 is observed for θ_1 , θ_2 and θ_3 respectively equal to 90, 45 and 95°. A least-squares refinement in reciprocal space leading to the best overlap and performed later, after the interpretation of the MIR map, led to angular values of 88.64, 41.53 and 85.08° for θ_1 , θ_2 and θ_3 . [The computation was performed by minimization of $(|F_o| - F_c)^2$, where F_o 's are the observed amplitudes for tRNA^{Asp} and F_c 's the calculated amplitudes using the tRNA^{Phe} model.] The results of the rotation function are roughly 10° from the solution giving the maximum overlap. This is most likely due to the

structural differences later observed, essentially the angular aperture of the two limbs of the L-shaped molecules, which is more open by roughly 20° in tRNA^{Asp}. The best fit results in a compromise between the best overlaps of each limb. Instead, the rotation function is dominated by the direction of the limbs which pack in continuous helices.

The observed agreement proved to be insufficient when the molecular-replacement approach was extended to the translation function. Despite numerous attempts using various functions, no successful solution could be found. A retrospective analysis after the answer became available from the MIR method confirmed the absence of solutions in the translation functions. The particular packing of tRNA^{Asp}, which results in infinite helices in two directions, might explain the lack of efficiency of these functions.

Multiple isomorphous replacement

Heavy-atom search. Due to the difficulty of selectively producing and identifying one crystal form from the other, two independent structure determinations had to be carried out by the MIR method. An additional difficulty was the interconvertibility of the two crystal forms which hampered the search for heavy-atom derivatives. A good example is the case of the Au derivative, which was difficult to obtain in form *A* since addition of Au salt in the mother liquor would drive form *A* crystals to an intermediate form

close to that of form *B*. As a consequence the phasing power of the Au derivative fades away between 4 and 4.5 Å resolution.

In our search for heavy-atom derivatives we were guided by the experience of previous studies on both yeast tRNA^{Phe} and tRNA^{Met}. Some of our attempts, the successful ones as well as others, are summarized in Table 5. Gd, Lu and La, used as sulfate salts, gave the best heavy-atom derivatives with a good isomorphism. A unique binding site was observed despite a large range of rare-earth concentration used. This site is similar to one of the two strong Sm binding sites in tRNA^{Phe}. The fact that none of the other binding sites observed in tRNA^{Phe} could be observed can now be explained essentially by a different conformation of the D loop (second strong binding site in tRNA^{Phe}) and/or by an important competition of ammonium ions (7*M*) for potential weak binding sites.

The second useful derivative was Au used as its ethylenediamine complex, whereas gold tetrachloride gave poor results. Two binding sites with different affinities were found. One is common to both crystal forms and is located in the pocket formed by the anticodon loop. The second site is near the contact area of the T loop of one tRNA and the CCA end of an adjacent molecule. From one crystal form to the other this second binding site moves by more than 3 Å. This movement is related to a conformational change of the tRNA molecule (Huong *et al.*, 1984).

Hg salts gave only poor derivatives because of the lack of isomorphism. Moreover, the simple binding site was on a crystallographic twofold axis, thus limiting the contribution of the Hg atoms to only half of the reflexions of the projection $h0l$ ($l = 2n$). This derivative, however, was very useful for the interpretation of the map since Hg atoms bind between two-fold-related anticodons, and brings useful chemical information.

Table 5 shows also some of the numerous unsuccessful attempts. Most of the markers were successfully used with tRNA^{Phe}. If the failures observed with Pb and Pt salts might only underline the absence of favorable binding sites in tRNA^{ASP} crystals, the situation is quite different with the Os derivative. In that case we followed the experimental conditions described by Rosa & Sigler (1974). tRNA^{ASP} crystals behave in a way similar to that described by the authors for yeast tRNA^{Met}. A light-blue color appeared after a few days, indicative of Os binding. Since no significant intensity changes could be noted the concentration of osmium-pyridine in the mother liquor was increased to 10⁻² *M* and then crystals became dark blue. An extensive washing of the crystals by Os-free mother liquor did not remove the color, clearly indicating the existence of a covalently bound derivative. After this treatment a diffraction data set was collected up to 5 Å resolution and

Table 5. Soaking experiments (some of the unsuccessful attempts are included)

Compound	Concentration (mM)	Soaking	Substitution	Isomorphism
Gd ₂ (SO ₄) ₃	5	48 h	1 site	good
	30	48 h		
Lu ₂ (SO ₄) ₃	30	48 h	1 site	good
La ₂ (SO ₄) ₃	30	48 h	1 site	good
Au(en) ₂ Cl ₃	2	1 week	2 sites	fair
NaAuCl ₄	2	1 week	2 sites	poor
<i>o</i> -Phenyl-Hg-Cl	1	1 week	1 site	poor
HgCl ₂	1	1 week	1 site	poor
OsO ₃ (py) ₂	10	3 weeks	no binding site*	
Pb(CH ₃) ₃ OAc	1	1 week	no substitution	
<i>cis</i> -Pt(NH ₂) ₂ Cl ₂	5	2 d-1 week	no substitution	
<i>trans</i> -Pt(NH ₂) ₂ Cl ₂	5	2 d-1 week	no substitution	

* For the Os derivative, crystals were colored (dark blue). Although the color remained after extensive washing of the crystals by mother liquor, no significant intensity change could be observed.

analyzed. No significant change could be detected. The only explanation we can give is that the reaction really occurs and Os binds to the terminal ribose of A76 as expected but with that part of the molecule disordered in the crystals, as confirmed by the subsequent refinement of the structure (Westhof, Dumas & Moras, 1985).

Refinement. Heavy-atom sites were located from difference Patterson maps. Absence of minor sites was checked on difference Fourier maps. The position and the occupancy of the heavy-atom sites together with their thermal motion were refined using a least-squares program (Adams *et al.*, 1969) implemented on our PDP minicomputer with only minor modifications.

Results of the refinement are summarized in Figs. 2(a) and 2(b) for forms *A* and *B*. The overall figure of merit to 3.5 Å is 0.60 for form *A* and 0.62 for form *B*. Heavy-atom coordinates are listed in Tables 6 and 7.*

Structural results

Electron density map

A 5 Å resolution electron density map phased with the two best derivatives (Gd and Au, figure of merit 0.72) enabled us to draw the shape and the boundaries of the tRNA^{ASP} molecule everywhere except for the corner of the molecule near the contact area of the

* Atomic coordinates and structure factors have been deposited with the Protein Data Bank, Brookhaven National Laboratory (Reference: 9TNA, R9TNASF), and are available in machine-readable form from the Protein Data Bank at Brookhaven or one of the affiliated centers at Cambridge, Melbourne or Osaka. The data have also been deposited with the British Library Lending Division as Supplementary Publication No. SUP 37016 (2 microfiche). Free copies may be obtained through The Executive Secretary, International Union of Crystallography, 5 Abbey Square, Chester CH1 2HU, England. At the request of the authors, the lists of coordinates and structure factors will remain privileged until 1 June 1987.

Table 6. Refinement of heavy-atom positions in crystal form A

3363 independent reflections were phased between 20 and 3.5 Å resolution. HgCl₂ yields a poorly isomorphous derivative, intermediate between A and B forms. The position of the Hg atom was then refined in both crystal forms.

Derivative	x	y	z	B (Å ²)	Relative occupancy	Resolution (Å)	Number of reflections
Lu ₂ (SO ₄) ₃	0.231	0.048	0.007	50	1.7	3.5	3114
Gd ₂ (SO ₄) ₃	0.234	0.048	0.007	43	2.5	3.5	3260
Au(en) ₂ Cl ₃	0.117	0.392	0.119	100	1.4	4.0	1911
	0.489	0.277	0.204	84	0.7		
Lu ₂ (SO ₄) ₃	0.227	0.048	0.007	42	1.0	3.5	3126
+ Au(en) ₂ Cl ₃	0.117	0.390	0.122	81	0.8		
HgCl ₂	0.500	0.292	0.250	56	0.4	4.0	1646

Table 7. Refinement of heavy-atom positions in crystal form B

3477 independent reflections were phased between 20 and 3.5 Å resolution.

Derivative	x	y	z	B (Å ²)	Relative occupancy	Resolution (Å)	Number of reflections
Gd ₂ (SO ₄) ₃	0.231	0.055	0.005	24	2.1	3.5	3321
Au(en) ₂ Cl ₂	0.147	0.358	0.124	100	4.8	4.0	1757
	0.479	0.279	0.197	100	1.8		
HgCl ₂	0.500	0.298	0.250	74	1.0	4.0	1949
Gd ₂ (SO ₄) ₃	0.231	0.052	0.006	49	1.7	3.5	2313
+ Au(en) ₂ Cl ₃	0.146	0.358	0.125	73	1.9		

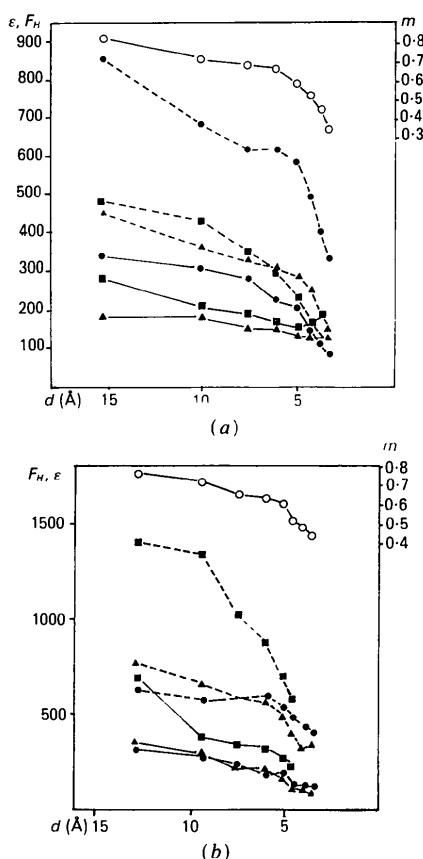


Fig. 2. Refinement statistics for (a) form A and (b) form B of tRNA^{Asp}. The limit of resolution for the phasing is 3.5 Å and the corresponding overall figure of merit is 0.60 for form A and 0.62 for form B. The figures show the contribution (F_H) of Gd (●), Au (■) and the mixed derivatives Lu + Au for form A (▲) and Gd + Au for form B. The r.m.s. lack of closures for each derivative are indicated by continuous lines. The scale is in arbitrary units.

D and T loops. In the crystals this portion of the tRNA comes close to the CCA end of another molecule brought there by the C-mode translation. This portion of the electron density map also contains one of the two Au binding sites and is therefore slightly perturbed. In this part of the map the problem of the boundaries was solved by topological considerations. The map clearly revealed the characteristic features⁴ of the tRNA structures: an L-shaped structure, helical stems and the anticodon loop.

As an example of the quality of the information at low resolution, three stereoscopic views of the map of form B crystals along the anticodon stem are shown in Fig. 3. The limit of resolution is 4.5 Å and corresponds to the limit of phasing power for the Au derivative (see Fig. 2). The overall figure of merit for this map is 0.70 with our program. It appears clearly that an atomic skeletal model could easily be built in the portion of the map which contains the helical stem. Some conformational ambiguities would certainly arise when attempting to construct the loop region. Fortunately most of the problems could be solved using the 3.5 Å resolution map. The positions of the phosphate atoms plotted as dots are extracted from the refined model (Westhof, Dumas & Moras, 1985). It is of interest to note that most of the phosphate atoms are not located at the center of the highest experimental electron density but at the border of it. Bases involved in base-pairing everywhere exhibit strong density. As an example two base pairs (29–41 and 31–39) are clearly visible in Fig. 3.

Kendrew model

A complete model was built in a Richard's box on a scale of 2 cm Å⁻¹ with Kendrew brass skeletal com-

ponents; a stereoview of this model is shown in Fig. 4. The heavy-atom binding sites are visualized by ping-pong balls at the metal location. The 3.5 Å electron density map was calculated at grid spacings of 0.75 Å and sectioned along the *y* axis. The higher-resolution data confirmed the first analysis. The complete ribose-phosphate backbone could be traced unambiguously everywhere except for a short fraction of the D loop where the density was weaker and perturbed, and near C75 and A76. In fact, the first model built was wrong in these regions. The lack of

clear and strong density near residues 18 and 19 was first attributed to poor phasing due to the proximity of a heavy-atom binding site, but we now think that local flexibility and dynamic disorder is a more likely explanation. In most places the phosphate group could be distinguished from the riboses, which appear as flat connecting densities between the phosphate bulbs. Almost all the bases had clear and strong flat electron density. Exceptions concern D19, C75, A76 and, to a lesser extent, C36. The first three named are among the few bases not involved in intra- or intermolecular tertiary interactions. The quality of the MIR map enabled us to interpret unequivocally most of the nucleotide conformations. One interesting part of the map is that of the anticodon loop and stem. This part of the molecule is obviously stabilized by the interactions between GUC anticodons of twofold-related molecules. The resulting electron density is strong.

Molecular packing

The packing of tRNA^{ASP} in orthorhombic forms is shown in Fig. 5. Two views along the *a* and *b* axes are drawn. A few major intermolecular contacts can be underlined, which are of general interest for nucleic acid interactions. The first, already mentioned, involves interactions between the anticodons of two molecules related by twofold crystallographic symmetry axes parallel to the direction of the *b* axis.

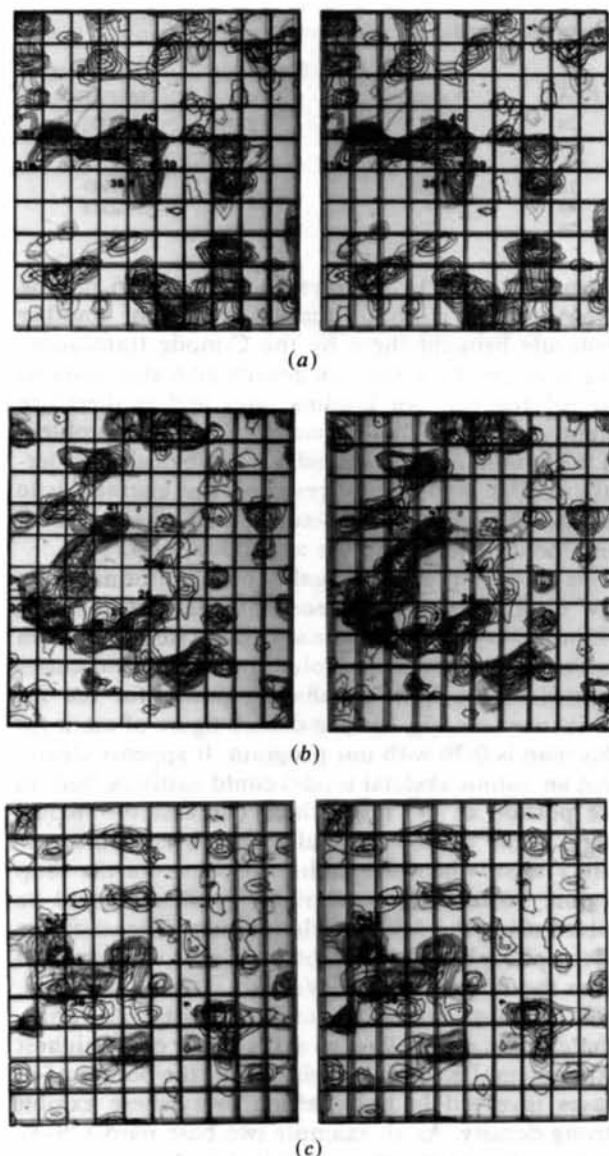


Fig. 3. Stereoviews of the MIR electron density map of form B crystals at 4.5 Å resolution. The limit corresponds to the limit of phasing power for the Au derivative. The overall figure of merit for this map is 0.70. The views are along the anticodon stem. The positions of the atoms represented by dots are those of the now refined model (Westhof *et al.*, 1985).

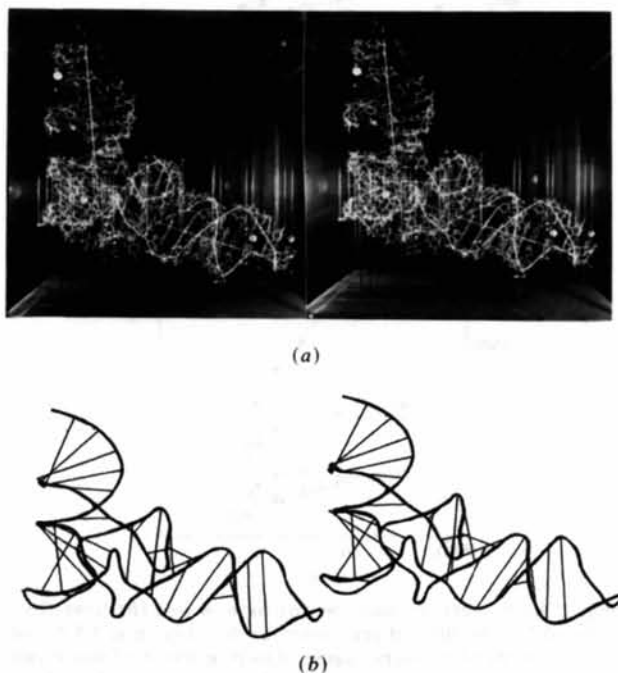


Fig. 4. Stereoviews of (a) the Kendrew skeletal model built from the 3.5 Å resolution MIR map and (b) the phosphate backbone without the CCA end in the same orientation; the base pairs are indicated by lines connecting the related phosphate groups.

The two GUC anticodons form two G-C base pairs and a U-U interaction across the twofold axis. The modified G at position 37 stacks on top of the G-C base pair, and stabilizes the association. The two related anticodons form a small helix which joins the two anticodon stems in a continuous helical stem. This is the first visualization of such an interaction which is a good model for the study of a codon-anticodon interaction. This association has already been studied in solution by Grosjean, De Henau & Crothers (1978) who showed that it was 10^4 times more stable than that between the anticodon and the corresponding codon alone. The conformation of the loop and the stabilizing effect of the stacking of G37 can explain the difference.

The second strong intermolecular contact is introduced by the C-mode translation which brings the T loop close to the CCA end of a neighboring molecule. As a result, two infinite and kinked helices are formed

roughly 110° apart and related by a twofold axis. A major consequence of this close contact is the steric hindrance of the corner of one molecule near position C56 toward the CCA of the other. The conformation of the single-stranded portion is certainly affected by the packing and cannot be helical. The fourth base G73 is still in its naturally stacked position, but C74, C75 and A76 are barely visible on the electron density map.

Another important intermolecular contact brings the anticodon stem and the D stem of one molecule on top of the T stem of another. The ribophosphate backbone comes in close proximity and interacts most probably through water or ammonium bridges. This is achieved through a twofold symmetry operation along the *a* axis.

A remarkable feature of yeast tRNA^{Asp} crystals is the existence of large solvent channels of approximately 18 Å diameter beside the anticodon loops. These holes are favorable for diffusing reagents. Chemical labelling of the anticodon region can thus be achieved within the crystal.

Comparison of crystal forms

Two sources of information are available for finding major differences between the two non-isomorphous crystal forms without waiting for the refinement of the two structures. The first source is the coordinates of the heavy-atom derivatives which underline a significant variation of the major Au binding site. The change of more than 3 Å is most likely correlated to an equivalent movement of the bound nucleotide. The binding site is located at the junction of the T loop of one molecule near residue 57 and the CCA end of another, C-mode related.

The second source of information is the averaged map computed from the two independent MIR maps. On this map all major features are conserved. The electron density is more contrasted for most of the molecule except for the D-loop region. For this part of the molecule the electron density is already very weak in the original maps, but the averaging washes out any significant signal, thus suggesting conformational differences in addition to an intrinsic flexibility indicated by the weakness of the original electron density.

The authors wish to thank Professor J. P. Ebel for continuous support, A. Lifchitz for the refinement of the superposition of tRNA^{Phe} and tRNA^{Asp} in reciprocal space and A. Wechsler for the preparation of Fig. 4.

References

- ADAMS, M. J., HAAS, D. J., JEFFERY, B. A., MCPHERSON, A. J., MERMALL, H. L., ROSSMANN, M. G., SCHEVITZ, R. W. & WONACOTT, A. J. (1969). *J. Mol. Biol.* **41**, 159-188.

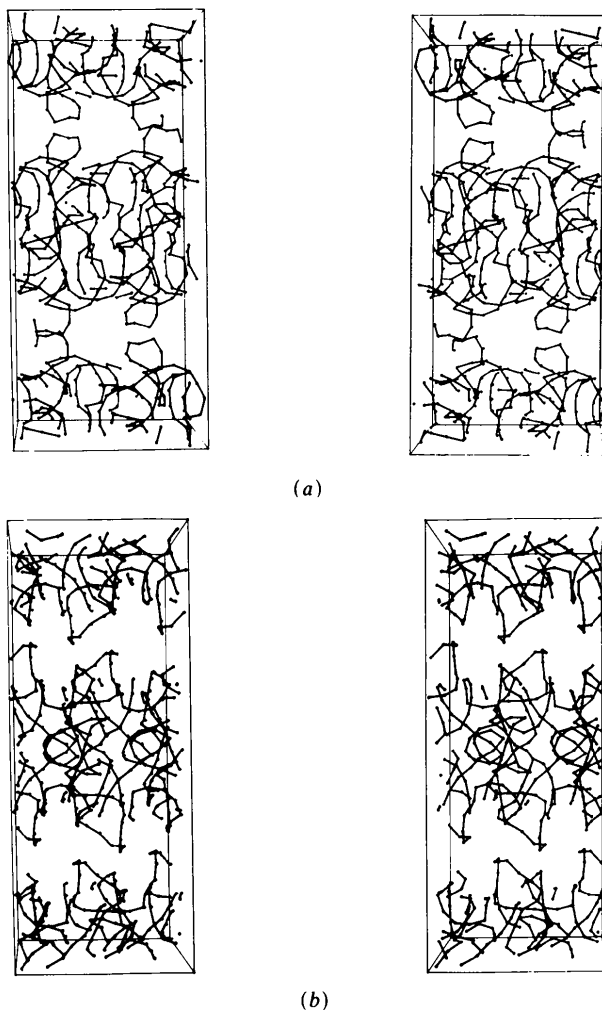


Fig. 5. Crystal packing of yeast tRNA^{Asp} viewed (a) along the *a* axis, and (b) along the *b* axis. Solvent channels near the anticodon loop regions are clearly visible.

- CROWTHER, R. A. (1972). *The Molecular Replacement Method*, edited by M. G. ROSSMANN, pp. 173-178. New York: Gordon and Breach.
- DOCK, A. C., LORBER, B., MORAS, D., PIXA, G., THIERRY, J. C. & GIEGÉ, R. (1984). *Biochimie*, **66**, 179-201.
- FISCHER, J., MORAS, D. & THIERRY, J. C. (1985). *J. Appl. Cryst.* **18**, 20-26.
- GANGLOFF, J., KEITH, G., EBEL, J. P. & DIRHEIMER, G. (1971). *Nature (London) New Biol.* **230**, 125-127.
- GIEGÉ, R., MORAS, D. & THIERRY, J. C. (1977). *J. Mol. Biol.* **115**, 91-96.
- GROSJEAN, H., DE HENAU, S. & CROTHERS, D. M. (1978). *Proc. Natl Acad. Sci. USA*, **75**, 610-616.
- HUONG, P. V., AUDRY, E., GIEGÉ, R., MORAS, D., THIERRY, J. C. & COMAROMOND, M. B. (1984). *Biopolymers*, **23**, 71-81.
- JACK, A., LADNER, J. E. & KLUG, A. (1976). *J. Mol. Biol.* **108**, 619-649.
- LADNER, J. E., JACK, A., ROBERTUS, J. D., BROWN, R. S., RHODES, D., CLARK, B. F. C. & KLUG, A. (1975). *Proc. Natl Acad. Sci. USA*, **72**, 4414-4418.
- LA ROSSA, R. & SÖLL, D. (1980). *Cell Monograph Series 2. Transfer RNA*, edited by S. ALTMANN, pp. 136-167. Cambridge and London: The MIT Press.
- MORAS, D., COMAROMOND, M. B., FISCHER, J., WEISS, R., THIERRY, J. C., EBEL, J. P. & GIEGÉ, R. (1980). *Nature (London)*, **286**, 669-674.
- NORTH, A. C. T., PHILLIPS, D. C. & MATHEWS, F. S. (1968). *Acta Cryst.* **A24**, 351-359.
- QUIGLEY, G. J., WANG, A., SEEMAN, N. C., SUDDATH, F. L., RICH, A., SUSSMAN, J. L. & KIM, S.H. (1975). *Proc. Natl Acad. Sci. USA*, **72**, 4866-4870.
- ROSA, J. J. & SIGLER, P. B. (1974). *Biochemistry*, **13**, 5102-5109.
- ROSSMANN, M. G. & BLOW, D. M. (1962). *Acta Cryst.* **15**, 24-31.
- SCHEVITZ, R. W., PODJARNY, A. D., KRISHNAMACHAR, N., HUGUES, T. T., SIGLER, P. B. & SUSSMAN, J. L. (1981). *Nature (London)*, **278**, 188-190.
- SCHIMMEL, P. R., SÖLL, D. & ABELSON, J. N. (1979). *Cold Spring Harbor Monogr. Ser.* **9A**, pp. 1-577.
- SPRINZL, M. & GAUSS, D. H. (1984). *Nucleic Acids Res.* **12**, 210-258.
- STOUT, C. D., MIZUNO, H., RAO, S. T., SWAMINATHAN, P., RUBIN, J., BRENNAN, T. & SUNDARALINGAM, M. (1978). *Acta Cryst.* **B34**, 1529-1544.
- SUSSMAN, J. L., HOLBROOK, S. R., WARRANT, R. W., CHURCH, G. M. & KIM, S. H. (1978). *J. Mol. Biol.* **123**, 607-674.
- WESTHOF, E., DUMAS, P. & MORAS, D. (1985). *J. Mol. Biol.* **184**, 119-145.
- WOO, N., ROE, B. & RICH, A. (1980). *Nature (London)*, **286**, 669-674.
- WRIGHT, H. T. (1982). *Topics in Nucleic Acid Structure. Part 2. New tRNA Crystal Structures Since Yeast tRNA^{Phe}*, edited by S. NEIDLE, pp. 137-171. London: Macmillan.

Acta Cryst. (1986). **B42**, 280-286

Phase Transition in 9-Hydroxyphenalenone at 255 K and Crystal Structure of the Ordered Phase at 215 K

By C. SVENSSON

Inorganic Chemistry 2, Chemical Center, University of Lund, S-221 00 Lund, Sweden

AND S. C. ABRAHAMS

AT&T Bell Laboratories, Murray Hill, New Jersey 07974, USA

(Received 16 September 1985; accepted 2 January 1986)

Abstract

9-Hydroxyphenalenone, $C_{13}H_8O_2$, $M_r = 196.205$, monoclinic, space group $P2_1$ below the reversible first-order phase transition at 255 K and space group $P2_1/c$ above. The thermal expansion has been followed from 145 to 360 K by single-crystal X-ray diffractometry. On heating, the a axis decreases sharply in length at the phase transition by 1.7%, the b axis increases smoothly, the c axis increases sharply by 1.5% and the angle β decreases sharply by 2.0%, with the volume expanding abruptly by 0.4%. Corresponding principal linear thermal-expansion coefficients at 145 K are -56 (19), 25 (8) and 192 (19) $\times 10^{-6} K^{-1}$ and at 360 K are -236 (9), 342 (5) and 283 (9) $\times 10^{-6} K^{-1}$. At 215 K $a = 9.091$ (4), $b = 28.581$ (7), $c = 7.011$ (3) Å and $\beta = 100.78$ (8)°, $V = 1789$ (1) Å³, $Z = 8$, $D_x = 1.456$, $D_m = 1.45$ (5) g cm⁻³

(298 K), λ (Mo $K\alpha_1$) = 0.70930 Å, $\mu = 0.89$ cm⁻¹, $F(000) = 816$. Crystal growth from benzene solution. Final $R = 0.0458$ for 5089 unaveraged independent hkl and $h\bar{k}l$ reflections measured at 215 K followed by least-squares refinement with anisotropic C and O, isotropic H-atom thermal amplitudes. Equivalent bond lengths in the four ordered independent molecules do not differ significantly. The average length of the intramolecular asymmetric hydrogen bond O...O is 2.490 (5) Å, with O-H = 1.12 (7) Å. The phase transition is associated with a 35° rotation in the molecular plane for one independent molecule: both this and one other molecule become disordered above the transition by an additional 120° rotation in the molecular plane. The configurational entropy change is calculated as 2.28 J mol⁻¹ K⁻¹, which compares well with the observed entropy change of 2.20(2) J mol⁻¹ K⁻¹.